

# Neutrino-pasta scattering: the opacity of nonuniform neutron-rich matter

C.J. Horowitz\* and M.A. Pérez-García†

*Nuclear Theory Center and Department of Physics, Indiana University, Bloomington, Indiana 47405*

J. Piekarewicz‡

*Department of Physics, Florida State University, Tallahassee, FL 32306*

(Dated: March 20, 2022)

Neutron-rich matter at subnuclear densities may involve complex structures displaying a variety of shapes, such as spherical, slablike, and/or rodlike shapes. These phases of the *nuclear pasta* are expected to exist in the crust of neutron stars and in core-collapse supernovae. The dynamics of core-collapse supernovae is very sensitive to the interactions between neutrinos and nucleons/nuclei. Indeed, neutrino excitation of the low-energy modes of the pasta may allow for a significant energy transfer to the nuclear medium, thereby reviving the stalled supernovae shock. The linear response of the nuclear pasta to neutrinos is modeled via a simple semi-classical simulation. The transport mean-free path for  $\mu$  and  $\tau$  neutrinos (and antineutrinos) is expressed in terms of the static structure factor of the pasta, which is evaluated using Metropolis Monte Carlo simulations.

PACS numbers:

## I. INTRODUCTION

Neutron-rich matter may have a complex structure at densities just below that of normal nuclei. This is because all conventional matter is *frustrated*. While nucleons are correlated at short distances by attractive strong interactions, they are anti-correlated at large distances because of the Coulomb repulsion. Often these short and large distance scales are well separated, so nucleons bind into nuclei that are segregated in a crystal lattice. However, at densities of the order of  $10^{13}$ – $10^{14}$  g/cm<sup>3</sup> these length scales are comparable [1]. Competition among these interactions (*i.e.*, *frustration*) becomes responsible for the development of complex structures with many possible nuclear shapes, such as spheres, cylinders, flat plates, as well as spherical and cylindrical voids [2]. The term *pasta phases* has been coined to describe these complex structures [1], and many calculations of their ground-state structure have already been reported [1, 2, 3, 4, 5, 6]. While the study of these pasta phases is interesting in its own right, it becomes even more so due to its relevance to the structure of the inner crust of neutron stars and to the dynamics of core-collapse supernovae.

Frustration, a phenomenon characterized by the existence of a very large number of low-energy configurations, emerges from the impossibility to simultaneously minimize all “elementary” interactions. Should a proton in the pasta join a nuclear cluster to benefit from the nuclear attraction or should it remain well separated to minimize the Coulomb repulsion? Frustration, a term that appears to have been coined in the late seventies [7, 8], is prevalent in complex systems ranging from magnetism [9, 10]

to protein folding [11]. In condensed-matter systems, frustration dates back to the 1950 study of Ising antiferromagnets on triangular lattices by Wannier [12]. Three antiferromagnetically coupled spins fixed to the sites of an equilateral triangle cannot minimize all interactions simultaneously: once two spins are anti-aligned, the third one cannot be antiparallel to both of them. Further, in Ref. [13] it has been shown that finding the true ground state—among the many metastable states—of a spin glass shares features in common with *NP-complete* problems, such as the *traveling salesman problem* of fame in the theory of combinatorial optimization [14]. Finally, because of the preponderance of low-energy states, frustrated systems display unusual low-energy dynamics.

Because of the complexity of the system, almost no work has been done on the low-energy dynamics of the pasta or on its response to weakly-interacting probes. In this paper we study the excitations of the pasta via a simple semi-classical simulation similar to those used to describe heavy-ion collisions. Heavy-ion collisions can produce hot, dense matter. However, by carefully heating the system and allowing it to expand, heavy-ion collisions can also study matter at low densities. Multi-fragmentation, the breakup of a heavy ion into several large fragments, shares many features with pasta formation, as they are both driven by the same volume, surface, and Coulomb energies. There have been several classical [15, 16] and quantum-molecular-dynamics (QMD) [17] simulations of heavy-ion collisions. These same approaches may be applied to the nuclear pasta by employing a simulation volume and periodic boundary conditions. One great advantage of such simulations is that one can study pasta formation in an unbiased way without having to assume particular shapes or configurations from the outset. While QMD has been used before to study the structure of the pasta [18, 19, 20], no calculations of its linear response to weakly-interacting probes (*e.g.*, neutrinos) have been reported.

---

\*Electronic address: horowit@indiana.edu

†Electronic address: mperezga@indiana.edu

‡Electronic address: jorgep@csit.fsu.edu

Neutrino interactions are crucial in the dynamics of core-collapse supernovae because neutrinos carry 99% of the energy. Neutrinos are initially trapped due to the large coherent neutrino-nucleus elastic scattering cross section. This trapping is important for the electron-per-baryon fraction  $Y_e$  of the supernova core, as it hinders any further conversion of electrons into neutrinos. However, with increasing density Coulomb interactions between ions lead to significant ion screening of neutrino-nucleus elastic scattering [21]. As the density is increased still further, the ions react to form nuclear pasta and one needs to calculate neutrino-pasta interactions.

In the pasta phase one can have coherent neutrino scattering from density contrasts, such as *Swiss cheese* like voids. Critical fluctuations could significantly increase the cross section, thereby greatly reducing the neutrino mean-free path. As the existence of many low-energy configurations is the benchmark of frustrated systems, one expects large configuration mixing among the various different pasta shapes. This mixing often leads to interesting low-energy collective excitations. As it will be shown later (see Fig. 2) at subnuclear densities of the order of  $10^{13}$  g/cm<sup>3</sup>, the pasta resembles a collection of spherical neutron-rich nuclei embedded in a dilute neutron gas. Neutron-rich nuclei with large neutron skins have *Pygmy giant resonances*, involving collective oscillations of the neutron skin against the symmetric core [22, 23]. We expect that the soft neutron-rich pasta will have many low-energy collective oscillations. This could provide important physics that is presently missing from core-collapse supernovae simulations. Neutrino excitation of the low-energy pasta modes may allow for a significant energy transfer to the nuclear medium, potentially reviving the stalled supernovae shock. To our knowledge, there have been no calculations of these effects. Note, however, that Reddy, Bertsch, and Prakash [24] have found that coherent neutrino scattering from a nonuniform kaon condensed phase greatly decreases the neutrino mean free path.

Present models of the equation of state for supernovae simulations, such as that of Lattimer and Swesty [25], describe the system as a liquid drop for a single representative heavy nucleus surrounded by free alpha particles, protons, and neutrons. One then calculates neutrino scattering from these constituents—by arbitrarily matching to a high-density uniform phase [26]. Unfortunately, this approximation is uncontrolled as it neglects many important interactions between nuclei. By simulating the pasta phase directly in the nucleon coordinates, one hopes to improve on this matching and to understand its limitations.

There is a duality between microscopic descriptions of the system in terms of nucleon coordinates and “macroscopic” descriptions in terms of effective nuclear degrees of freedom. Thus, a relevant question to pose is as follows: when does a neutrino scatter from a nucleus and when does it scatter from an individual nucleon? At the Jefferson Laboratory a similar question is studied; when,

*i.e.*, at what momentum transfer, does a photon couple to a full hadron and when to an individual quark? Models of the quark/hadron duality have provided insight on how descriptions in terms of hadron degrees of freedom can be equivalent to descriptions in terms of quark coordinates [27]. Here we are interested in nucleon/nuclear duality, that is, how can nuclear models incorporate the main features of microscopic nucleon descriptions?

The manuscript has been organized as follows. In Sec. II the semi-classical formalism is introduced. A very simple (perhaps minimal) model is employed that contains the essential physics of frustration. The linear response of the pasta to neutrino scattering, in the form of a static structure factor, is discussed in Sec. III. Results are presented in Sec. IV, while conclusions and future directions are reserved to Sec. V.

## II. FORMALISM

In this section we introduce a classical model that while simple, contains the essential physics of frustration. That is, competing interactions consisting of a short-range nuclear attraction and a long-range Coulomb repulsion. We model a charge-neutral system of electrons, protons, and neutrons. The electrons are assumed to be a degenerate free Fermi gas of density  $\rho_e = \rho_p$  and the nucleons interact via a classical potential. The only quantum aspects of the calculation are the use of an effective temperature and effective interactions to simulate effects associated with quantum zero-point motion. Of course more elaborate models are possible and these will be presented in future contributions. For these first simulations we adopted a very simple version that displays the essential physics of nucleons clustering into pasta in a transparent form. Moreover, this simple model facilitates simulations with a relatively large numbers of particles, a feature that is essential to estimate and control finite-size effects.

The total potential  $V_{\text{tot}}$  energy is assumed to be a sum over two-body interactions  $V_{ij}$  of the following form:

$$V_{\text{tot}} = \sum_{i < j} V(i, j), \quad (1)$$

where the “elementary” two-body interaction is given by

$$V(i, j) = ae^{-r_{ij}^2/\Lambda} + \left[ b + c\tau_z(i)\tau_z(j) \right] e^{-r_{ij}^2/2\Lambda} + V_c(i, j). \quad (2)$$

Here the distance between the particles is denoted by  $r_{ij} = |\mathbf{r}_i - \mathbf{r}_j|$  and the isospin of the  $j$ th particle is  $\tau_z(j) = 1$  for a proton and  $\tau_z(j) = -1$  for a neutron. The model parameters  $a$ ,  $b$ ,  $c$ , and  $\Lambda$  will be discussed below. Suffices to say that the above interaction includes the characteristic intermediate-range attraction and short-range repulsion of the nucleon-nucleon ( $NN$ ) force. Further, the isospin dependence of the potential insures that while pure neutron matter is unbound, symmetric nuclear matter is bound appropriately. Finally, a screened Coulomb

interaction of the following form is included:

$$V_c(i, j) = \frac{e^2}{r_{ij}} e^{-r_{ij}/\lambda} \tau_p(i) \tau_p(j), \quad (3)$$

where  $\tau_p(j) = (1 + \tau_z(j))/2$  and  $\lambda$  is the screening length that results from the slight polarization of the electron gas. That is, the relativistic Thomas-Fermi screening length is given by

$$\lambda = \frac{\pi}{e} \left( k_F \sqrt{k_F^2 + m_e^2} \right)^{-1/2}, \quad (4)$$

Note that the electron Fermi momentum has been defined by  $k_F = (3\pi^2 \rho_e)^{1/3}$  and  $m_e$  is the electron mass [28, 29]. Unfortunately, while the screening length  $\lambda$  defined above is smaller than the length  $L$  of our simulation box, it is not significantly smaller (unless a prohibitively large number of particles is used). Therefore, to control finite-size effects we were forced to arbitrarily decrease the value of  $\lambda$  (see Sec. IV).

The simulations are carried out in a canonical ensemble with a fixed number of particles  $A$  at a temperature  $T$ . The volume  $V$  at a fixed baryon density  $\rho$  is simply  $V = A/\rho$ . To minimize finite-size effects we use periodic boundary conditions, so that the distance  $r_{ij}$  is calculated from the  $x$ ,  $y$ , and  $z$  coordinates of the  $i$ th and  $j$ th particles as follows:

$$r_{ij} = \sqrt{[x_i - x_j]^2 + [y_i - y_j]^2 + [z_i - z_j]^2}, \quad (5)$$

where the periodic distance, for a cubic box of side  $L = V^{1/3}$ , is given by

$$[l] = \text{Min}(|l|, L - |l|). \quad (6)$$

The potential energy defined in Eq. (1) is independent of momentum. Therefore, the partition function for the system factors into a product of a partition function in momentum space—that plays no role in the computation of momentum-independent observables—times a coordinate-space partition function of the form

$$Z(A, T, V) = \int d^3 r_1 \cdots d^3 r_A \exp(-V_{\text{tot}}/T). \quad (7)$$

Note that the 3-dimensional integrals are performed over the simulation volume  $V$ .

The average energy of the system  $\langle E \rangle = \langle K \rangle + \langle V_{\text{tot}} \rangle$  is made of kinetic ( $K$ ) and potential ( $V_{\text{tot}}$ ) energy contributions. As the (momentum-independent) interactions have no impact on momentum-dependent quantities, the expectation value of the kinetic energy reduces to its classical value, that is,

$$\langle K \rangle = \frac{3}{2} AT. \quad (8)$$

In turn, the expectation value of the potential energy may be computed from the coordinate-space partition

function as follows:

$$\langle V_{\text{tot}} \rangle = \frac{1}{Z(A, T, V)} \int d^3 r_1 \cdots d^3 r_A V_{\text{tot}} \exp(-V_{\text{tot}}/T). \quad (9)$$

In summary, a classical system has been constructed with a total potential energy given as a sum of two-body momentum-independent interactions [see Eq. (2)]. Any momentum-independent observable of interest can be calculated from the partition function [Eq. (7)], which we evaluate via Metropolis Monte-Carlo integration [30].

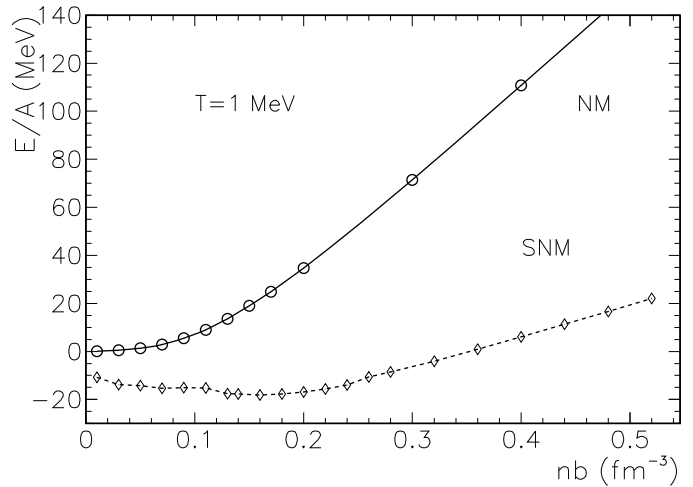


FIG. 1: Energy per particle for symmetric (dashed line) and for pure-neutron matter (solid) versus baryon density  $nb$  at a temperature of  $T=1$  MeV.

We now return to discuss the choice of model parameters. The constants  $a$ ,  $b$ ,  $c$ , and  $\Lambda$  in the two-body interaction Eq. (2) were adjusted—approximately—to reproduce the following bulk properties: a) the saturation density and binding energy per nucleon of symmetric nuclear matter, b) (a reasonable value for) the binding energy per nucleon of neutron matter at saturation density, and c) (approximate values for the) binding energy of a few selected finite nuclei. The temperature was arbitrarily fixed at 1 MeV for all the calculations. Note that the parameter set employed in these calculations (and displayed in Table I) has yet to be carefully optimized. We reiterate that for these first set of simulations, the interaction is sufficiently accurate to describe the essential physics of the pasta. Indeed, this is illustrated in Fig. 1 and Table II. In Fig. 1 the average potential energy versus density at a temperature of  $T = 1$  MeV is displayed for a simulation of symmetric nuclear matter containing  $A=400$  particles and, as is customary, assuming no Coulomb interactions. Also shown in the figure is the potential energy for pure neutron matter calculated with  $N=200$  particles. In the case of finite nuclei (also calculated at  $T=1$  MeV) the full Coulomb interaction is included using a screening length  $\lambda$  much larger than the resulting root-mean-square radius of the nucleus. Simulations based on a Metropolis Monte-Carlo algorithm were

TABLE I: Model parameters used in the calculations.

$a$	$b$	$c$	$\Lambda$
110 MeV	-26 MeV	24 MeV	1.25 fm <sup>2</sup>

TABLE II: Binding energy per nucleon for various closed shell nuclei. Note that all energies are in MeV and that the Monte-Carlo results include only  $\langle V_{\text{tot}} \rangle$ .

Nucleus	Monte Carlo $\langle V_{\text{tot}} \rangle$	Experiment
<sup>16</sup> O	-7.56 ± 0.01	-7.98
<sup>40</sup> Ca	-8.75 ± 0.03	-8.45
<sup>90</sup> Zr	-9.13 ± 0.03	-8.66
<sup>208</sup> Pb	-8.2 ± 0.1	-8.45

used to compute the average potential energy, starting with nucleons distributed uniformly in a sphere with a radius comparable to the expected size of the nucleus; this sphere was placed in the center of a very large box. Results of the simulations and comparison with experimental values have been collected in Table II. Note that the simulation results are for the potential energy only. If the kinetic energy per nucleon ( $3T/2$ ) is added to these values, the nuclei in Table II would be slightly underbound. Furthermore, finite nuclei are only metastable in this semiclassical approximation. Nucleons can evaporate over a very long time scale. However, this is not expected to significantly impact the pasta phases since these already have free nucleons.

### III. NEUTRINO SCATTERING

The model is used to describe neutrino scattering from nonuniform neutron-rich matter. As neutrino interactions play a predominant role in core-collapse supernovae, one is interested in understanding how the neutrinos diffuse and how do they exchange energy. In this first paper we focus on the transport mean free path for  $\nu_\mu$  and  $\nu_\tau$ , which lack charged-current interactions at low energies. Their mean-free path is dominated by neutral current neutrino-nucleon scattering.

The free-space cross section for neutrino-nucleon elastic scattering is given by

$$\frac{d\sigma}{d\Omega} = \frac{G_F^2 E_\nu^2}{4\pi^2} [c_a^2(3 - \cos\theta) + c_v^2(1 + \cos\theta)] , \quad (10)$$

where  $G_F$  is the Fermi coupling constant,  $E_\nu$  the neutrino energy and  $\theta$  the scattering angle. Note that this equation neglects weak magnetism and other corrections of order  $E_\nu/M$ , with  $M$  the nucleon mass [31].

In the absence of weak magnetism, the weak neutral current  $J_\mu$  of a nucleon has axial-vector ( $\gamma_5\gamma_\mu$ ) and vector  $\gamma_\mu$  contributions. That is,

$$J_\mu = c_a\gamma_5\gamma_\mu + c_v\gamma_\mu . \quad (11)$$

The axial coupling constant is,

$$c_a = \pm \frac{g_a}{2} \quad (g_a = 1.26) , \quad (12)$$

with the + sign for neutrino-proton and the - sign for neutrino-neutron scattering. The weak charge of a proton  $c_v$  is suppressed by the weak-mixing (or Weinberg) angle  $\sin^2\theta_W = 0.231$ ,

$$c_v = \frac{1}{2} - 2\sin^2\theta_W = 0.038 \approx 0 . \quad (13)$$

In contrast, the weak charge of a neutron is both large and insensitive to the weak-mixing angle:  $c_v = -1/2$ . The transport mean-free path  $\lambda_t$  is inversely proportional to the transport cross section  $\sigma_t$  and is given by the following expression:

$$\sigma_t = \int d\Omega \frac{d\sigma}{d\Omega} (1 - \cos\theta) = \frac{2G_F^2 E_\nu^2}{3\pi} (5c_a^2 + c_v^2) . \quad (14)$$

The weighting factor  $(1 - \cos\theta)$  included in the definition of the transport cross section favors large-angle scattering, as momentum is transferred more efficiently into the medium. As a result, the axial-vector contribution  $c_a^2$  dominates the cross section. Assuming that the scattering in the medium is the same as in free space, the transport mean-free path becomes

$$\lambda_t = (\rho_p\sigma_t^p + \rho_n\sigma_t^n)^{-1} . \quad (15)$$

Here  $\rho_p(\rho_n)$  is the proton(neutron) density and  $\sigma_t^p(\sigma_t^n)$  is the transport cross section for scattering from a proton(neutron).

If nucleons cluster tightly into nuclei or into pasta, then the scattering from different nucleons could be coherent. This will significantly enhance the cross section as it would be proportional to the *square* of the number of nucleons [32]. The contribution from the vector current is expected to be coherent. Instead, the strong spin and isospin dependence of the axial current should reduce its coherence. This is because in nuclei—and presumably in the pasta—most nucleons pair off into spin singlet states (note that in the nonrelativistic limit the nucleon axial-vector current becomes  $\gamma_5\gamma_\tau z \rightarrow -\sigma\tau_z$ ). Therefore, in this paper we focus exclusively on coherence effects for the vector current.

Coherence is important in x-ray scattering from crystals. Because the x-ray wavelength is comparable to the inter-particle spacing, one needs to calculate the relative phase for scattering from different atomic planes and then sum over all planes. Neutrino-pasta scattering involves a similar sum because the neutrino wavelength is comparable to the inter-particle spacing and even to the inter-cluster spacing. Therefore, one must calculate the relative phase for neutrino scattering from different nucleons and then add their contribution coherently. This procedure is embodied in the static structure factor  $S(q)$ .

The dynamic response of the system to a probe of momentum transfer  $\mathbf{q}$  and energy transfer  $\omega > 0$  that couples to the weak charge density  $\hat{\rho}(\mathbf{q})$  is given by [28]

$$S(\mathbf{q}, \omega) = \sum_{n \neq 0} \left| \langle \Psi_n | \hat{\rho}(\mathbf{q}) | \Psi_0 \rangle \right|^2 \delta(\omega - \omega_n), \quad (16)$$

where  $\omega_n$  is the energy difference between the excited state  $|\Psi_n\rangle$  and the ground state  $|\Psi_0\rangle$ . In linear response theory, namely, assuming that the process can be treated in lowest order (an excellent approximation for neutrino scattering) the cross section can be directly related to the dynamic response of the system. In the case that the individual excited states may not be resolved, then one integrates over the energy transfer  $\omega$  to obtain the static structure factor. Here we define the static structure factor *per neutron* as follows:

$$S(\mathbf{q}) = \frac{1}{N} \int_0^\infty S(\mathbf{q}, \omega) d\omega = \frac{1}{N} \sum_{n \neq 0} \left| \langle \Psi_n | \hat{\rho}(\mathbf{q}) | \Psi_0 \rangle \right|^2, \quad (17)$$

with the weak vector-charge density given by

$$\rho(\mathbf{q}) = \sum_{i=1}^N \exp(i\mathbf{q} \cdot \mathbf{r}_i), \quad (18)$$

where the sum in Eq. (18) is only over neutrons.

The cross section *per neutron* for neutrino scattering from the whole system is now given by

$$\frac{1}{N} \frac{d\sigma}{d\Omega} = S(\mathbf{q}) \frac{G_F^2 E_\nu^2}{4\pi^2} \frac{1}{4} (1 + \cos\theta). \quad (19)$$

Note that the weak charge of the nucleon ( $c_p \approx 0$  for protons and  $c_n = -1/2$  for neutrons) has been incorporated into the above cross section, so that the normalization of the weak vector-charge density is  $\rho(q=0) = N$ . Further, Eq. (19) is the cross section per neutron obtained from Eq. (10) (with  $c_a = 0$ ) multiplied by  $S(\mathbf{q})$ . This indicates that  $S(\mathbf{q})$  embodies the effects from coherence. Finally, note that the momentum transfer is related to the scattering angle through the following equation:

$$q^2 = 2E_\nu^2(1 - \cos\theta). \quad (20)$$

Two assumptions have been made in the derivation of Eq. (19). First, no contribution from the axial current to the cross section has been included, because nucleons pair into spin-zero states. Second, the excitation energy transferred to the nucleons is small and we have summed over all possible excitation energies.

The static structure factor has important limits. A particularly useful form in which to discuss them invokes completeness on Eq. (17). That is,

$$S(\mathbf{q}) = \frac{1}{N} \left( \langle \Psi_0 | \hat{\rho}^\dagger(\mathbf{q}) \hat{\rho}(\mathbf{q}) | \Psi_0 \rangle - \left| \langle \Psi_0 | \hat{\rho}(\mathbf{q}) | \Psi_0 \rangle \right|^2 \right). \quad (21)$$

The last term in the above expression represents the elastic form factor of the system, which only contributes at  $q = 0$ . In the limit of  $q \rightarrow 0$ , the weak charge density [Eq. (18)] becomes the number operator for neutrons  $\hat{\rho}(q=0) = \hat{N}$ , so that the static structure factor reduces to,

$$S(q=0) = \frac{1}{N} \left( \langle \hat{N}^2 \rangle - \langle \hat{N} \rangle^2 \right). \quad (22)$$

Thus, the  $q \rightarrow 0$  limit of the static structure factor is related to the fluctuations in the number of particles, or equivalently, to the density fluctuations. These fluctuations are, themselves, related to the compressibility and diverge at the critical point [33]. To discuss the large  $q$  limit, Eq. (18) is substituted into Eq. (21) to yield

$$S(\mathbf{q}) = \frac{1}{N} \left( \sum_{i,j}^N \langle \Psi_0 | \exp(i\mathbf{q} \cdot \mathbf{r}_{ij}) | \Psi_0 \rangle - \left| \langle \Psi_0 | \hat{\rho}(\mathbf{q}) | \Psi_0 \rangle \right|^2 \right), \quad (23)$$

In the  $q \rightarrow \infty$  limit, all the terms in the sum with  $i \neq j$ , as well as the second term in the above expression, oscillate to zero. This only leaves the  $i = j$  terms, which there are  $N$  of them so that

$$S(q \rightarrow \infty) = 1. \quad (24)$$

This result indicates that if the neutrino wavelength is much shorter than the inter-particle separation, the neutrino only resolves one nucleon at a time. This corresponds to quasielastic scattering where the cross section per nucleon in the medium is the same as in free space.

One can calculate the static structure factor from the neutron-neutron correlation function which is defined as follows:

$$g(\mathbf{r}) = \frac{1}{N\rho_n} \sum_{i \neq j}^N \langle \Psi_0 | \delta(\mathbf{r} - \mathbf{r}_{ij}) | \Psi_0 \rangle. \quad (25)$$

The two-neutron correlation function “asks” (and “answers”) the following question: if one “sits” on a neutron, what is the probability of finding another one a distance  $|\mathbf{r}|$  away. The correlation function is normalized to one at large distances  $g(r \rightarrow \infty) = 1$ ; this corresponds to the average density of the medium. The static structure factor is obtained from the Fourier transform of the two-neutron correlation function. Comparing with Eq. (23) this yields,

$$S(\mathbf{q}) = 1 + \rho_n \int d^3r (g(\mathbf{r}) - 1) \exp(i\mathbf{q} \cdot \mathbf{r}). \quad (26)$$

The  $i = j$  terms in Eq. (23) gives the leading 1 in the above expression, while the elastic form factor  $|\langle \Psi_0 | \hat{\rho}(\mathbf{q}) | \Psi_0 \rangle|^2$  yields the  $-1$  in the integrand of Eq. (26).

To obtain the transport cross section we proceed, as in Eq. (10), to integrate the angular-weighted cross section  $d\sigma/d\Omega(1 - \cos\theta)$  over all angles. That is,

$$\sigma_t = \frac{1}{N} \int d\Omega \frac{d\sigma}{d\Omega} (1 - \cos\theta) = \langle S(E_\nu) \rangle \sigma_t^0. \quad (27)$$

Note that the free neutron cross  $\sigma_t^0$  follows directly from Eq. (14) in the limit of  $c_a \equiv 0$ ,

$$\sigma_t^0 = \frac{G_F^2 E_\nu^2}{6\pi}. \quad (28)$$

Further, the angle averaged static structure factor has been defined as follows:

$$\langle S(E_\nu) \rangle \equiv \frac{3}{4} \int_{-1}^1 dx (1-x^2) S(q(x, E_\nu)), \quad (29)$$

where the static structure factor  $S(q)$  depends on neutrino energy and angle through Eq. (20), that is,  $q^2 = 2E_\nu^2(1-x)$  with  $x = \cos\theta$ . Using Eq. (26) and switching the orders of integration, this can be written as

$$\langle S(E_\nu) \rangle = 1 + \frac{4\pi\rho_n}{E_\nu^2} \int_0^\infty dr f(2E_\nu r) (g(r) - 1). \quad (30)$$

Note that the following function has been introduced

$$f(t) = 72(\cos t + t \sin t - 1)/t^4 - 6(5 \cos t + t \sin t + 1)/t^2. \quad (31)$$

Finally, the transport mean free path ( $\lambda_t = 1/\sigma_t \rho_n$ ) is given by

$$\lambda_t^{-1} = \sigma_t^0 \rho_n \langle S(E_\nu) \rangle. \quad (32)$$

In this way  $\langle S(E_\nu) \rangle$  describes how coherence modifies the mean-free path. In the next section, simulation results for the two-neutron correlation function, the static structure factor, and the angle averaged static structure factor will be presented.

#### IV. RESULTS

In this section we present our simulation results. As an example of a typical low-density condition we consider a subnuclear density of  $\rho = 0.01 \text{ fm}^{-3}$  (about 1/16 of normal nuclear density), a temperature  $T = 1 \text{ MeV}$ , and an electron fraction of  $Y_e = 0.2$ . Proto-neutron stars have electron fractions that start out near 1/2 and drop with time, so  $Y_e = 0.2$  represents a typical neutron-rich condition. Monte-Carlo simulations for a total of  $A = 4000$  particles ( $N = 3200$ ,  $Z = 800$ ) have been performed. Because of the many competing minima, a significantly larger system would take an unreasonably long time to thermalize on a modest work station (see details below).

The simulation volume for the above conditions consists of a cube of length  $L = 73.7 \text{ fm}$ . While this value is larger than the electron screening length  $\lambda = 26.6 \text{ fm}$  [see Eq. (4)], it is not sufficiently larger. Indeed, to minimize finite-size effects in a simulation with periodic boundary conditions one would like  $\exp(-L/(2\lambda)) \ll 1$ . Clearly, this condition is not adequately satisfied. Therefore, in an effort to minimize the contamination from finite-size effects, we reduce the electron screening length—arbitrarily—to the following value:

$$\lambda \equiv 10 \text{ fm}. \quad (33)$$

This value for  $\lambda$  is adopted hereafter for all of our simulations (see also [18]). This smaller screening length decreases slightly the Coulomb interaction at large distances, which could promote the growth of slightly larger clusters. However, we do not expect this decrease in  $\lambda$  to qualitatively change our results. We note that  $\lambda$  is still larger than the typical size of a heavy nucleus.

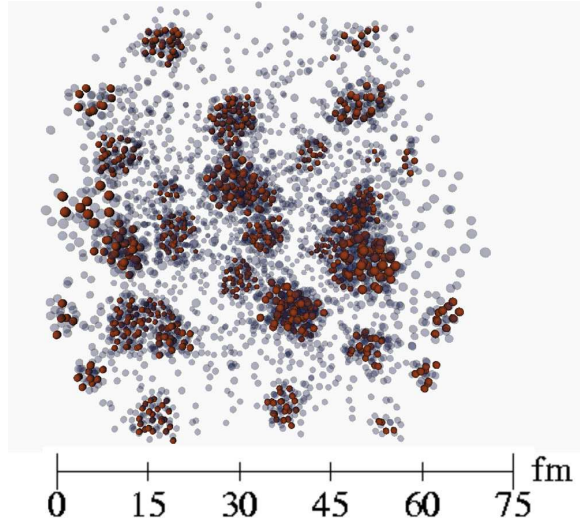


FIG. 2: (Color online) Monte-Carlo snapshot of a configuration of  $N = 3200$  neutrons (light gray circles) and  $Z = 800$  protons (dark red circles) at a baryon density of  $\rho = 0.01 \text{ fm}^{-3}$ , a temperature of  $T = 1 \text{ MeV}$ , and an electron fraction of  $Y_e = 0.2$ . 3D imaging courtesy of the FSU Visualization Laboratory.

By far, the most time consuming part of the simulation is producing suitable initial conditions. The simulations are started with the  $A = 4000$  nucleons randomly distributed throughout the simulation volume. Next, we perform a total of about 325,000 Metropolis sweeps starting at the higher temperature of  $T = 2 \text{ MeV}$  and reducing the temperature until eventually reaching the target temperature of  $T = 1 \text{ MeV}$ , in a “poor’s-man” attempt at simulated annealing. Note that a Metropolis sweep consists of a single trial move for each of the  $A = 4000$  particles in this system. We call this procedure cooking the pasta.

Results in this section are based on a statistical average of the final 50,000 sweeps. This yields a potential energy of  $-5.385 \pm 0.003 \text{ MeV/A}$ . A sample configuration of the 4000 particles is shown in Fig. 2. The protons are strongly correlated into clusters (“nuclei”) as are a large number of neutrons. In addition, there is a low density neutron gas between the clusters. At this density it may be reasonable to think of the system as a high-density liquid of “conventional” nuclei immersed in a dilute neutron gas. A great virtue of the simulation is that one does not have to arbitrarily decide which nucleons cluster in nuclei and which ones remain in the gas. These “decisions” are being answered dynamically. Further, one can

calculate modifications to nuclear properties due to the interactions. In a future work we plan to compare our simulation results to some conventional nuclear models.

Protons moving between clusters face a Coulomb barrier. This may inhibit the thermalization process and with it the formation of larger clusters. This could increase our results for  $S(\mathbf{q})$ . To test the thermalization of the pasta, our Metropolis Monte Carlo configuration was evolved further via molecular dynamics for a total time of 46,500 fm/c. The molecular dynamics calculations will be described in future work. This led to an increase in the peak of  $S(q)$  by only about 10 percent. Although these molecular dynamics results did not reveal a large secular change in the system with time, we caution that our cooking procedure may not have converged to the true thermal-equilibrium state. The static structure factor  $S(q)$  may still change with additional Metropolis Monte Carlo or molecular dynamics evolution.

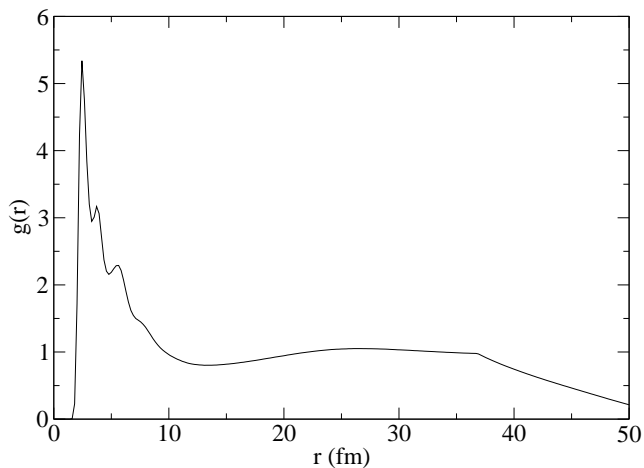


FIG. 3: Neutron-neutron correlation function at a temperature of  $T = 1$  MeV, an electron fraction of  $Y_e = 0.2$ , and a baryon density of  $\rho = 0.01$  fm $^{-3}$ . These results show large finite-size effects beyond  $r = L/2 = 36.9$  fm.

The neutron-neutron correlation function  $g(r)$  is displayed in Fig. 3. The two-neutron correlation function is calculated by histogramming the relative distances between neutrons. The correlation function is very small at short distances because of the hard core in our  $NN$  interaction. At intermediate distances  $g(r)$  shows a large broad peak between  $r = 2$  fm and  $r \simeq 10$  fm. This corresponds to the other neutrons bound into a cluster. Superimposed on this broad peak one observes three (or four) sharper peaks corresponding to nearest, next-to-nearest, and next-to-next-to-nearest neighbors. These structures describe two-neutron correlations within the same cluster. At larger distances, between 10 and 20 fm, the correlation function shows a modest dip below one, suggesting that the attractive  $NN$  interaction has shifted some neutrons from larger to smaller distances in order to form

the clusters. Alternatively, Coulomb repulsion makes it less likely to find two clusters separated by these radii. Finally, there is an abrupt drop in  $g(r)$  at a distance corresponding to half the value of the simulation length ( $r = L/2 = 36.9$  fm) caused by finite-size effects. We note that under our assumptions of periodic boundary conditions,  $g(r)$  is identically zero for  $r > \sqrt{3}L/2$ .

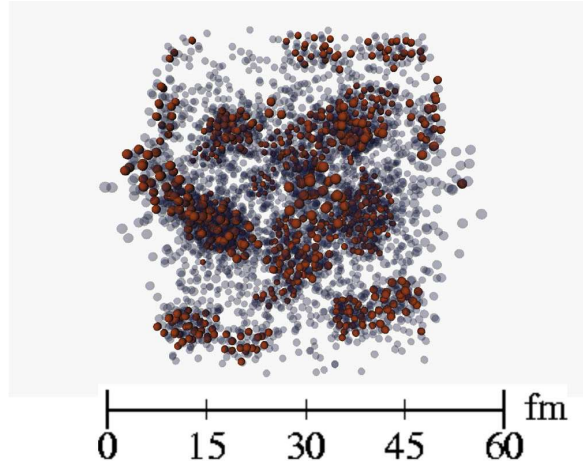


FIG. 4: (Color online) Monte-Carlo snapshot of a configuration of  $N = 3200$  neutrons (light gray circles) and  $Z = 800$  protons (dark red circles) at a baryon density of  $\rho = 0.025$  fm $^{-3}$ , a temperature of  $T = 1$  MeV, and an electron fraction of  $Y_e = 0.2$ . 3D imaging courtesy of the FSU Visualization Laboratory.

Increasing the density can change the nature of the pasta. Figure 4, shows a sample configuration of 4000 particles at a density of  $0.025$  fm $^{-3}$ . Note that although the density has increased, both the temperature and the electron fraction have remained fixed at  $T = 1$  MeV and  $Y_e = 0.2$ , respectively. At a density of  $\rho = 0.025$  fm $^{-3}$  (about 1/6 of normal nuclear-matter saturation density) the spherical clusters of Fig. 2 start to coalesce into *cylindrical-like* structures. The system appears to be segregated into high-density regions of cylindrical nuclei immersed in a dilute neutron gas. As we continue to perform additional simulations, high-quality renderings of nucleon configurations for a variety of densities, temperatures, and electron fractions will be developed.

To compute the static structure factor  $S(q)$ , one numerically transforms the two-neutron correlation function, as indicated in Eq. (26). However, because of finite-size effects we truncate the integral at  $r = L/2$  and assume  $g(r) \equiv 1$  for  $r > L/2$ . This procedure yields the results displayed in Fig. 5. There is a modest peak in  $S(q=0)$  due to density fluctuations. Of course, the number of neutrons in our simulation remains fixed, yet fluctuations can take neutrons across the  $r = L/2$  cutoff and these fluctuations will contribute to the value of  $S(q)$  at  $q = 0$ .

The error bars in Fig. 5 are statistical only, based on the last 50,000 sweeps. We caution that there may be finite-size effects at small momentum transfers. The box

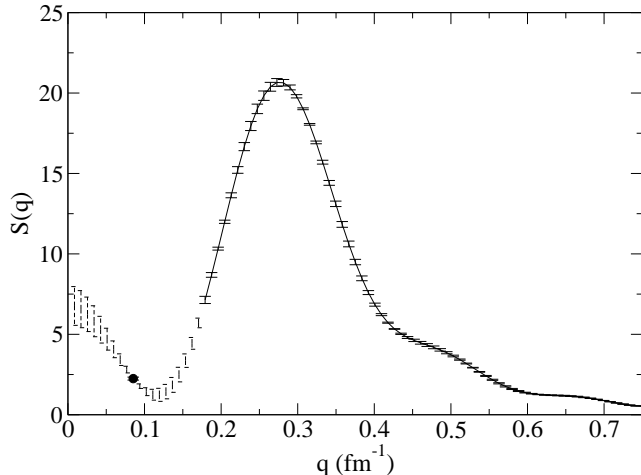


FIG. 5: Static structure factor  $S(\mathbf{q})$  versus momentum transfer  $q$  at a temperature of  $T = 1$  MeV, an electron fraction of  $Y_e = 0.2$ , and a baryon density of  $\rho = 0.01$  fm $^{-3}$ . The error bars are statistical only. Finite size effects may be important at small  $q$  as indicated by the dotted error bars.

size for our simulation at  $\rho = 0.01$  fm $^{-3}$  is  $L = 73.7$  fm. This corresponds to a minimum momentum transfer of

$$q_{\min} \approx \frac{2\pi}{L} = 0.085 \text{ fm}^{-1}. \quad (34)$$

Momentum transfers smaller than  $q_{\min}$  correspond to wavelengths larger than the simulation volume, so our results for  $q \lesssim 2q_{\min}$  may be sensitive to finite-size effects. Indeed, for  $q \lesssim 2q_{\min}$  the static structure factor was observed to change significantly from one Metropolis run to the next. To indicate the sensitivity of our results to finite-size effects, Fig. 5 displays the static structure factor in the  $q \leq 2q_{\min}$  region with dotted error bars. Note that the point  $q = q_{\min}$  has been signaled out in Fig. 5 to indicate that it is more stable from one Metropolis run to the next, because the weak vector-charge density [Eq. (18)] evaluated at  $\mathbf{q} = q_{\min}\hat{\mathbf{q}}$  is invariant under a translation of the system by a distance  $L$  along  $\hat{\mathbf{q}}$ .

The static structure factor displays a large peak at  $q \approx 0.3$  fm $^{-1}$ , corresponding to coherent scattering from many neutrons bound into a single cluster. At smaller momentum transfers,  $q \approx 0.2$  fm $^{-1}$ ,  $S(\mathbf{q})$  decreases because of ion screening. Here the neutrino wavelength is so long that it probes multiple clusters. These other clusters screen the weak charge and reduce the response. At momentum transfers larger than  $q \approx 0.3$  fm $^{-1}$ , the static structure factor decreases with increasing  $q$ . This is the effect of the cluster form factor. As the momentum transfer increases the neutrino can no longer scatter coherently from all the neutrons in a cluster because of the clusters extended size. Thus, the observed peak in  $S(\mathbf{q})$  develops as a trade off between ion screening, which favors large  $q$ , and the cluster form factor, which favors small  $q$ .

In summary, one can divide the response of the pasta into the following regions. At low-momentum transfers ( $q \lesssim 0.2$  fm $^{-1}$ ) the response is dominated by ion screening and density fluctuations. For momentum transfers in the region  $q = 0.2 - 0.4$  fm $^{-1}$  one observes coherent scattering from the pasta. At the larger momenta of  $q = 0.4 - 1$  fm $^{-1}$ , the falling response reflects the pasta form factor. Finally, the large momentum transfer region above  $q = 1$  fm $^{-1}$  corresponds to quasielastic scattering from nearly free neutrons, as  $S(q \rightarrow \infty) = 1$  [see Eq. (24)].

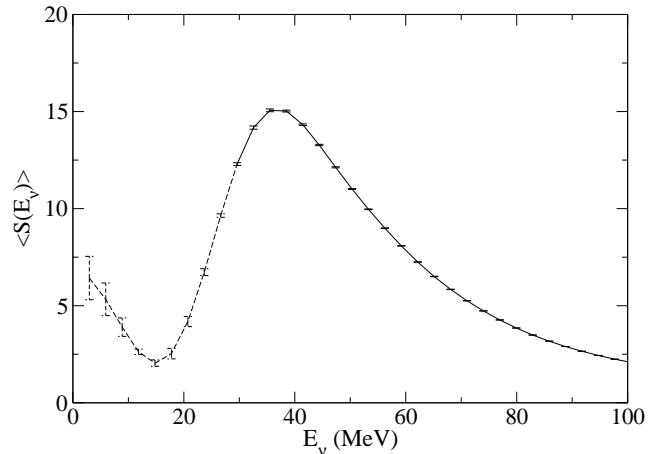


FIG. 6: Angle averaged static structure factor  $\langle S(E_\nu) \rangle$  versus neutrino energy  $E_\nu$  at a temperature of  $T = 1$  MeV, an electron fraction of  $Y_e = 0.2$ , and a baryon density of  $\rho = 0.01$  fm $^{-3}$ . The error bars are statistical only, see text.

The angle averaged structure factor  $\langle S(E_\nu) \rangle$  [defined in Eq. (29)] is shown in Fig. 6. Note that the integral in Eq. (30) was also truncated at  $r = L/2$  because of finite-size effects. The averaged structure factor shows a broad peak for neutrino energies near 40 MeV. Indeed, the transport cross section is significantly enhanced by coherence effects for neutrino energies from about 20 to 80 MeV. The impact of this coherence on the neutrino mean-free path [Eq. (32)] is displayed in Fig. 7. Also shown in the figure is the mean-free path obtained by ignoring coherence effects by setting  $\langle S(E_\nu) \rangle = 1$  in Eq. (32). Coherence significantly reduces the mean-free path for neutrino energies in the range  $E_\nu = 15 - 120$  MeV. Again, finite size effects may be important for low neutrino energies.

## V. CONCLUSIONS

Neutron-rich matter is expected to have a complex structure at subnuclear densities. Complex pasta phases may result from frustration through the competition between an attractive nuclear interaction and the Coulomb repulsion. Neutrino interactions with the pasta may

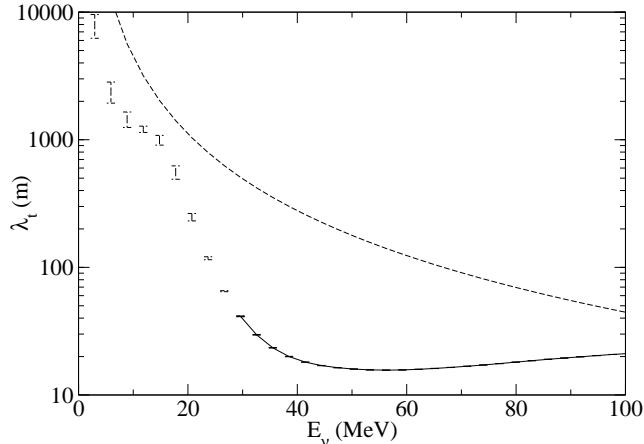


FIG. 7: Transport mean-free path  $\lambda_t$  for  $\nu_\mu$  or  $\nu_\tau$  versus neutrino energy  $E_\nu$  at a baryon density of  $\rho=0.01 \text{ fm}^{-3}$ , a temperature of  $T=1 \text{ MeV}$ , and an electron fraction of  $Y_e=0.2$ . The solid line and error bars include full coherence effects while the dashed line is obtained by using  $\langle S(E) \rangle = 1$  in Eq. (32). Error bars are statistical only. Finite size effects may be important for low  $E_\nu$  as indicated by the dotted error bars.

be important for properties of core-collapse supernovae, such as its electron fraction.

In this work we have employed a semi-classical model to simulate the dynamics of the pasta phase of neutron-rich matter. Although our model is very simple, it nonetheless retains the crucial physics of frustration. Using a Metropolis Monte-Carlo algorithm, the partition function was computed for a system of 4000 nucleons at a given temperature and density. We find that almost all protons and most of the neutrons cluster into “nuclei” that are surrounded by a dilute neutron gas.

Observables computed in our simulations included the neutron-neutron correlation function. This calculation was implemented by constructing a histogram of all relative neutron distances. The two-neutron correlation function  $g(r)$  gives the probability of finding a neutron at a distance  $r$  away from a reference neutron. A large peak in  $g(r)$  at intermediate distances ( $r=2-10 \text{ fm}$ ) is found. This reflects the presence of the other neutrons in the cluster.

The static structure factor  $S(\mathbf{q})$ , a fundamental observable obtained from the Fourier transform of the two-neutron correlation function, describes the degree of coherence for neutrino-nucleon elastic scattering. For small momentum transfers,  $S(\mathbf{q})$  describes density fluctuations and ion screening. In this region the neutrino wavelength is longer than the average inter-cluster separation, thereby allowing other clusters to screen the weak charge of a given cluster. At momentum transfers of approximately  $q=0.2-0.4 \text{ fm}^{-1}$ , the static structure factor develops a large peak, associated to the coherent scatter-

ing from all the neutrons in the cluster. This coherence is responsible for a significant reduction in the neutrino mean-free path. To our knowledge, these represent the first consistent calculation of the neutrino mean-free path in nonuniform neutron-rich matter.

However, much remains to be done. First, one needs to focus on the thermalization of our simulations. It is difficult to insure that the system has reached thermal equilibrium because the Coulomb barrier hinders the motion of individual protons. Second, one must further investigate the impact of finite-size effects and the simple treatment of long-range Coulomb interactions on our simulations. This may require simulations with larger numbers of particles, as it is difficult to fit a long-wavelength neutrino into the present simulation volume. Third, while we have focused here on the vector part of the weak-neutral-current response, because it can be greatly enhanced by coherence, one should extend the study to the axial-vector (or spin) response, as it dominates the scattering when it is coming from uncorrelated nucleons. Further, one should also calculate charged-current interactions in nonuniform matter. Finally, in the present contribution no effort was made to optimize the  $NN$  interaction. While it may be advantageous to do so, any *accurately calibrated* interaction must retain the essential features of frustration. Moreover, more sophisticated interactions that include momentum and/or density dependence will significantly increase the computational demands. At present, we are checking our results against more sophisticated simulations using molecular dynamics, studying finite size effects in larger simulations, exploring the temperature and density dependence of our results, and calculating the dynamical response. These results will be presented in a future contribution [34].

## Acknowledgments

We acknowledge useful discussions with Wolfgang Bauer, Adam Burrows, Vladimir Dobrosavljevic, Thomas Janka, Sanjay Reddy, Pedro Schlottmann, Romualdo de Souza, and Victor Viola. C.J.H. thanks the Aspen Center for Physics, the Max Planck Institute for Astrophysics, and the Institute for Nuclear Theory at the University of Washington for their hospitality. M.A.P.G. acknowledges partial support from Indiana University and FICYT. J.P. thanks David Banks and the staff at the FSU Visualization Laboratory for their help. This work was supported in part by DOE grants DE-FG02-87ER40365 and DE-FG05-92ER40750.

- 
- [1] D. G. Ravenhall, C. J. Pethick, and J. R. Wilson, Phys. Rev. Lett. **50**, 2066 (1983).
- [2] M. Hashimoto, H. Seki, and M. Yamada, Prog. Theor. Phys. **71**, 320 (1984).
- [3] R. Williams and S. E. Koonin, Nucl. Phys. **A435**, 844 (1985).
- [4] K. Oyamatsu, Nucl. Phys **A561**, 431 (1993).
- [5] K. Sumiyoshi, K. Oyamatsu, and H. Toki, Nucl. Phys **A595**, 327 (1995).
- [6] C. P. Lorenz, D. G. Ravenhall, and C. J. Pethick, Phys. Rev. Lett. **70**, 379 (1993).
- [7] G. Toulouse, Commun. Phys. **2**, 115 (1977).
- [8] J. Villain, Jour. Phys. C **10**, 1717 (1977).
- [9] R. Liebmann, *Statistical Mechanics of Periodic Frustrated Ising Systems*, vol. 251 (Springer-Verlag, Berlin Heidelberg, 1986).
- [10] H. T. Diep, *Magnetic Systems with Competing Interactions* (World Scientific, Singapore, 1994).
- [11] C. J. Camacho, Phys. Rev. Lett. **77**, 2324 (1996).
- [12] G. H. Wannier, Phys. Rev. **79**, 357 (1950).
- [13] S. Kirkpatrick and D. Sherrington, Phys. Rev. B **17**, 4384 (1978).
- [14] C. H. Papadimitriou and K. Kenneth Steiglitz, *Combinatorial Optimization: Algorithms and Complexity* (Dover, Mineola, New York, 1998).
- [15] A. R. Bodmer, C. N. Panos, and A. D. MacKellar, Phys. Rev. C **22**, 1025 (1980).
- [16] T. J. Schlagel and V. R. Pandharipande, Phys. Rev. C **36**, 162 (1987).
- [17] G. Peilert, J. Randrup, H. Stocker, and W. Greiner, Phys. Lett. B **260**, 271 (1991).
- [18] T. Maruyama, K. Niita, K. Oyamatsu, T. Maruyama, S. Chiba, and A. Iwamoto, Phys. Rev. C **57**, 655 (1998).
- [19] G. Watanabe, K. Sato, K. Yasuoka, and T. Ebisuzaki, Phys. Rev. C **68**, 035806 (2003), nucl-th/0308007.
- [20] G. Watanabe, K. Sato, K. Yasuoka, and T. Ebisuzaki (2003), nucl-th/0311083.
- [21] C. J. Horowitz, Phys. Rev. D **55**, 4577 (1997).
- [22] M. Igashira, H. Kitazawa, H. Komano, and N. Yamamuro, Nucl. Phys. **A457**, 301 (1986).
- [23] D. Vretenar, N. Paar, P. Ring, and G. A. Lalazissis, Phys. Rev. C **63**, 047301 (2001), nucl-th/0009057.
- [24] S. Reddy, G. Bertsch, and M. P. Prakash, Phys. Lett. **B475**, 1 (2000).
- [25] J. M. Lattimer and F. D. Swesty, Nucl. Phys. **A535**, 331 (1992).
- [26] M. Liebendoerfer, O. E. B. Messer, A. Mezzacappa, S. W. Bruenn, C. Y. Cardall, and F. K. Thielemann (2002), astro-ph/0207036.
- [27] S. Jeschonnek and J. W. Van Orden, Phys. Rev. D **65**, 094038 (2002), and references therein.
- [28] A. L. Fetter and J. D. Walecka, *Quantum Theory of Many-Particle Systems* (McGraw-Hill, New York, 1971).
- [29] S. A. Chin, Ann. of Phys. **108**, 301 (1977).
- [30] N. Metropolis, A. Rosenbluth, M. Rosenbluth, A. Teller, and E. Teller, Jour. Chem Phys. **21**, 1087 (1953).
- [31] C. J. Horowitz, Phys. Rev. D **65**, 043001 (2002).
- [32] D. Z. Freedman, D. N. Schramm, and D. L. Tubbs, Annu. Rev. Nucl. Sci. **27**, 167 (1977).
- [33] P. A. Egelstaff, *An Introduction to the Liquid State* (Academic Press, New York, 1967).
- [34] C. J. Horowitz, M. A. Pérez-García, and J. Piekarewicz, in preparation.